TECTONICS, VOL. 10, NO. 6, PAGES 1187-1203, DECEMBER 1991

SEISMICITY AND FAULT INTERACTION, SOUTHERN SAN JACINTO FAULT ZONE AND ADJACENT FAULTS, SOUTHERN CALIFORNIA: IMPLICATIONS FOR SEISMIC HAZARD

Mark D. Petersen,[1] Leonardo Seeber,[2] Lynn R. Sykes,[1] John L. Nábělek,[3] John G. Armbruster,[2] Javier Pacheco,[1] and Kenneth W. Hudnut[4]

Abstract. The southern San Jacinto fault zone is characterized by high seismicity and a complex fault pattern that offers an excellent setting for investigating interactions between distinct faults. This fault zone is roughly outlined by two subparallel master fault strands, the Coyote Creek and Clark-San Felipe Hills faults, that are located 2 to 10 km apart and are intersected by a series of secondary cross faults. Seismicity is intense on both master faults and secondary cross faults in the southern San Jacinto fault zone. The seismicity on the two master strands occurs primarily below 10 km; the upper 10 km of the master faults are now mostly quiescent and appear to rupture mainly or solely in large earthquakes. Our results also indicate that a considerable portion of recent background activity near the April 9, 1968, Borrego Mountain rupture zone (M_L=6.4) is located on secondary faults outside the fault zone. We name and describe the Palm Wash fault, a very active secondary structure located about 25 km northeast of Borrego Mountain that is oriented subparallel to the San Jacinto fault system, dips approximately 70° to the northeast, and accommodates right-lateral shear motion. The Vallecito Mountain cluster is another secondary feature delineated by the recent seismicity and is characterized by swarming activity prior to nearby large events on the master strand. The 1968 Borrego Mountain and the April 28, 1969, Coyote Mountain (M_L=5.8) events are examples of earthquakes with aftershocks and subevents on these secondary and master faults. Mechanisms from those earthquakes and recent seismic data for the period 1981 to 1986 are not simply restricted to strike-slip motion; dip-slip motion is also indicated. Teleseismic body waves (long-period P and SH) of the 1968 and 1969 earthquakes were inverted simultaneously for source mechanism, seismic moment, rupture history, and centroid depth. The complicated waveforms of the 1968 event (M_o=1.2 x 10^{19} N m) are interpreted in terms of two subevents; the first caused by right-lateral strike-slip motion in the mainshock along the Coyote Creek fault and the second by a rupture located about 25 km away from the master fault. Our waveform inversion of the 1969 event indicates that strike-slip motion predominated, releasing a seismic moment of 2.5 x 10^{17} N m. Nevertheless, the right-lateral nodal plane of the focal mechanism is significantly misoriented (20°) with respect to the master fault, and hence the event is not likely to be associated with a rupture on that fault. From this and other examples in southern California, we conclude that cross faults may contribute significantly to seismic hazard and that interaction between faults has important implications for earthquake prediction.

INTRODUCTION

The southern California section of the Pacific and North American plate boundary is a complex shear zone located in a transitional tectonic environment. Extensional tectonics are associated with the opening of the Gulf of California to the south and the Basin and Range province to the east, while compressional tectonics elevate the Transverse Ranges to the north and west. Thus deformation is complex in the Salton Sea region. Displacement is primarily accommodated by major fault systems that trend northwest: the San Andreas, San Jacinto, and Elsinore fault zones (Figure 1).

On a regional scale the San Jacinto fault is a classical example of a fault zone characterized by steeply dipping dextral faults [e.g., Dibblee, 1954, 1984], intense seismicity [e.g., Hamilton, 1972], and long lineaments observed on satellite images of the area [e.g., Rockwell et al., 1990]. The zone is defined by two dextral master faults that trend northwest, subparallel to the North American-Pacific plate boundary (Figure 1). These master strands are from 2 to 10 km apart and define the width of the fault zone.

Shearing along the southern San Jacinto fault zone is accommodated not only by right-lateral master faults that trend northwest but also by shorter secondary right-lateral faults that are subparallel to the master faults and by left-lateral cross faults that trend northeast [Nicholson et al., 1986; Seeber and Nicholson, 1986]. Cross faults are also observed as prominent features in geologic [e.g., Sharp, 1972], seismic [e.g., Nicholson et al., 1986], geomorphologic [e.g., Rockwell et al., 1990], and gravity data (e.g., P.A. Cowie and L. Seeber, unpublished manuscript, 1990). Many cross faults are short and terminate against the master faults. Surface structure [e.g., Sharp, 1972], reflection and refraction data (e.g., Bond et al., unpublished manuscript, 1990, and Severson [1987]), and seismicity [e.g., Thatcher and Hamilton, 1973; Hamilton, 1972] indicate that thrust and normal faults have been active as were detachment faults,

[1]Department of Geological Sciences and Lamont-Doherty Geological Observatory of Columbia University, Palisades, New York.

[2]Lamont-Doherty Geological Observatory of Columbia University, Palisades, New York.

[3]College of Oceanography, Oregon State University, Corvallis.

[4]Seismological Laboratory, California Institute of Technology, Pasadena.

Paper number 91TC01240
0278-7407/91/91TC-01240$10.00

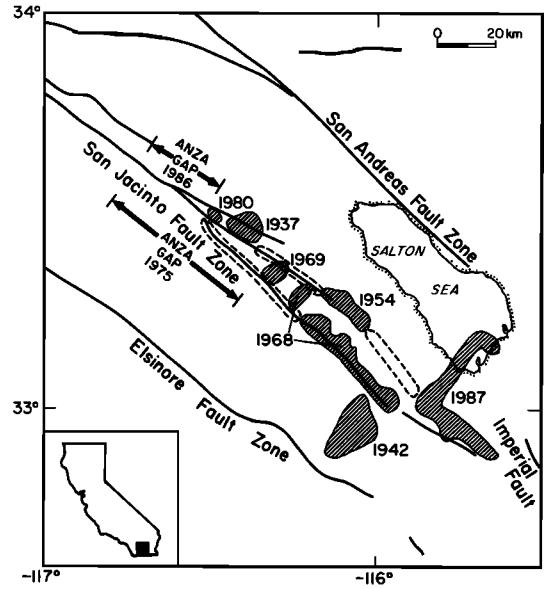

Fig. 1. Index map of southern California master faults including the San Andreas, San Jacinto, and Elsinore fault zones. Relocated aftershock zones from Sanders et al. [1986] for the large ($M \geq 5.5$) events in 1937, 1942, 1954, 1968, 1969, 1980, 1987 are shown with diagonal striped pattern. Seismic gaps identified in this study are shown as open dashed circles. Definitions of the Anza seismic gap from Sanders et al. [1986] and Thatcher et al. [1975] are also indicated. Distance scale is in upper right corner.

i.e., near-horizontal dipping faults at midcrustal depths.

Master faults slip more rapidly and tend to be longer than individual cross faults [e.g., Hudnut et al., 1989b]. Large ($M > 5.5$) earthquakes in the study area ruptured master faults in 1987 (M_L=6.6), 1968 (M_L=6.4), 1954 (M_L=6.2), and possibly in 1937 (M_L=6.0; Figure 1). Although secondary faults often rupture in bursts of microseismicity [Sanders and Kanamori, 1984], they may also rupture in moderate ($4 < M < 5.5$) to large ($M > 5.5$) earthquakes. The first event of the 1987 Superstition Hills sequence (M_L=6.2) occurred on a left-lateral, northeast-striking cross fault and was followed by a larger right-lateral rupture on the northwest-striking Superstition Hills fault (M_L=6.6) about 12 hours later. Other cross faults may have ruptured in 1969 (M_L=5.8; this paper) and 1942 (M_L=6.5 [Doser, 1990]; see Figure 1).

This research, in conjunction with previous work [Nicholson et al., 1986], suggests that an understanding of secondary faulting is important for at least two reasons. First, significant strain is being accommodated by slip on secondary faults, in particular cross faults. The contribution to the regional strain by secondary faults is accompanied by a significant contribution to earthquake hazard. Second, the stress-strain fields of master faults may be coupled with those of cross faults. Cross faults can segment the master fault by creating barriers to the rupture propagation and thereby control the characteristic length of rupture. They may also trigger events on master faults, as demonstrated by the 1987 Superstition Hills events [Hudnut et al., 1989a]. These secondary faults may therefore control the time-space distribution of earthquakes on master faults. Patterns of seismicity on secondary faults may indicate when rupture along a master fault will occur.

In the northernmost portion of the April 9, 1968, Borrego Mountain rupture zone, where several cross faults have been mapped, aftershocks trend northeast [Hamilton, 1972]. Cross-fault activity on the Inspiration Point fault is thought to have caused a barrier to the northward propagation of the 1968 rupture [Seeber and Nicholson, 1986]. The waveforms of this earthquake were investigated extensively [Wyss and Hanks, 1972; Burdick and Mellman, 1976; Heaton and Helmberger, 1977; Ebel and Helmberger, 1982; Kikuchi and Kanamori, 1985]. Rupture during the earthquake centered primarily along the Coyote Creek fault, displacing sediments in the vicinity of the epicenter a maximum of 38 cm horizontally in a right-lateral sense [Clark, 1972]. Aftershocks, however, occurred not only on the Coyote Creek fault but also on other structures in a wide and complex zone [Hamilton, 1972].

The Coyote Mountain earthquake (M_L 5.8) occurred about a year later (April 28, 1969) and just to the north of the 1968 surface rupture (Figure 1). While the Borrego Mountain aftershocks extended over most of the upper 10 km of the fault [Hamilton, 1972], the Coyote Mountain aftershocks were concentrated at depths between 10 and 12 km [Thatcher and Hamilton, 1973]. Reverse and strike-slip mechanisms were reported from analysis of aftershock focal mechanisms of the 1968 and 1969 events [Allen and Nordquist, 1972; Hamilton, 1972; Thatcher and Hamilton, 1973]. Surface ruptures with left-lateral displacement were also observed on fractures following the 1968 rupture [Clark, 1972]. Many of these fractures were observed near Borrego Mountain; the fractures had maximum left-lateral offsets of between 30 and 40 mm and many trended northeasterly. In addition, paleomagnetic data [Scheuing and Seeber, 1989] and geodetic data [Hudnut and Seeber, 1987] give evidence for substantial Plio-Quaternary block rotation near the 1969 rupture, which would imply large left-lateral offsets on cross faults that bound the blocks. Our results indicate that the 1969 earthquake may have occurred on a cross fault. Thus the 1968 and 1969 earthquake sequences involve a complex series of ruptures on both master and secondary faults.

The purpose of this paper is to examine the relationship between secondary and master faults along the southern San Jacinto fault zone. Our research includes a study of the spatial and temporal aspects of the present seismicity, waveform inversions for the 1968 and 1969 events, and an analysis of focal mechanisms produced from short-period seismic data. We show a complex pattern of

recent seismic activity that differs drastically from the pattern of aftershocks following larger events that rupture along master faults. Interseismic activity along the master faults tends to occur around the rims of major ruptures in a pattern that resembles the seismicity along the Loma Prieta segment of the San Andreas fault [Plafker and Galloway, 1989]. Prominent seismicity outside the San Jacinto fault zone is associated with a newly discovered secondary fault that we name the Palm Wash fault (located 25 km east of the epicenter of the Borrego Mountain earthquake) and with a cluster of activity beneath the Vallecito Mountains (located 15 km west of the 1968 epicenter). Secondary fault activity may be an important precursory signal that may be useful for short to intermediate term prediction of large earthquakes on master faults.

RESULTS OF THE 1968 BORREGO MOUNTAIN AND 1969 COYOTE MOUNTAIN WAVEFORM INVERSIONS

Several authors have studied the waveforms of the 1968 earthquake [Hamilton, 1972; Burdick and Mellman, 1976; Ebel and Helmberger, 1982; Kikuchi and Kanamori, 1985]. All of these authors agree that high moment release occurred over 6 s, in what we refer to as the first subevent, with orientation that is similar to the strike of the master fault. Some authors have, however, also suggested that seismic moment was released after the first subevent in subsequent events. Burdick and Mellman [1976] suggested that the moment was released in three subevents, from three distinct and separate regions and not simply along the master fault. Kikuchi and Kanamori [1985] identify the moment release after the first subevent but suggest that this moment is insignificant in decreasing the residuals in the fits of the waveform data. Thus in this paper we reanalyze the 1968 event and complete statistical tests to determine whether the 1968 event released significant moment in a second subevent on a secondary fault. We also analyze the resolution of each resultant parameter for the second subevent since we are interested in understanding secondary faults and their relationship to master faults.

The 1969 earthquake has been associated with a rupture on the mainstrand Coyote Creek fault. The aftershock distribution is dispersed in space, and several of the aftershocks were probably not located on the master fault. If the 1969 earthquake occurred along a secondary fault instead of along the master fault, the length of the Anza seismic gap may be considerably longer than was previously thought. Thus we analyze the 1969 earthquake to determine if the waveforms give some indication of whether the rupture occurred along the master fault or some other secondary fault.

Data and Method

Long-period P and SH waves of both the 1968 and 1969 earthquakes that were recorded by the World-Wide Standardized Seismological Network (WWSSN) were hand digitized and interpolated at an interval of 0.5 s. An excellent azimuthal distribution of stations located between distances of 30° and 90° was available for both events; this is essential for well-constrained nodal planes.

In our inversion, observed seismograms are compared to synthetic seismograms in a least squares sense to estimate the source mechanism (strike, dip, rake), centroid depth, scalar moment, and shape of the source-time function [Nábělek, 1984]. Synthetic body wave seismograms consist of direct P and S arrivals as well as reflections from the free surface. Complicated body waves are modeled by longer source duration and additional source energy and are treated as the superposition of subevent waveforms. The source-time function is represented by a series of overlapping triangles. The elementary theoretical seismograms are produced by convolving the source function with geometrical spreading, anelastic attenuation ($t^*=1$ for P waves, 4 for SH waves), instrument response, and source-receiver Green's functions. We use arrival times from short-period seismograms to constrain the start time of the P wave inversion window.

Results of Waveform Inversion for the 1968 Earthquake

Initially, a single source-time function 6 s long was used in the inversion for the 1968 Borrego Mountain earthquake and was sufficient to resolve most features in the observed seismograms. The mechanisms, waveforms, and source-time function of the 1968 event are shown in Figure 2 and the parameters and their uncertainties in Table 1. The mechanism of the first subevent, obtained from this inversion, represents motion on the Coyote Creek fault and is consistent with other published results and aftershock patterns [Hamilton, 1972; Burdick and Mellman, 1976; Ebel and Helmberger, 1982; Kikuchi and Kanamori, 1985]. Our preferred nodal plane strikes nearly northwest (311°), consistent with the observed orientation of surface ruptures along the master fault [Clark, 1972] and dips steeply northeast (78°), in agreement with the aftershock distribution [Hamilton, 1972]. The first subevent released a seismic moment of 9.2×10^{18} N m at 10 km centroid depth, near the base of the seismogenic zone inferred from the current seismicity and aftershocks [Doser and Kanamori, 1986].

We introduced a second subevent 12 s after the first subevent; synthetic seismograms with two subevents yielded lower residuals than seismograms with a single-event source. Although Kikuchi and Kanamori [1985] concluded that the presence of a second subevent is not significant, a paired t test [Huang et al., 1986] indicates that the existence of a second subevent is significant in lowering residuals at a 99% confidence level. A line source, however, did not lower residuals with respect to a point source. Hence we inverted for the source parameters

of the second pulse of energy as an independent point source.

Parameter resolution of the second subevent (Figure 3) is more uncertain than for the first subevent. While strike, dip, and slip parameters for the second event of the inversion exhibit narrow well-defined minima, depth, distance, and azimuth of the two centroids are not well constrained by this waveform inversion. The second subevent may be less resolved than the first subevent because of three reasons. First, the second subevent comes in the coda of the first large subevent. Second, the second subevent has a low moment release rate and therefore did not excite as much high-frequency energy. The short-period records indicate a second subevent, but it is difficult to interpret the onset of that subevent. Third, the second subevent has low amplitude with respect to the first subevent. These three factors cause a low signal-to-noise ratio for the second subevent that causes difficulty in resolution of source parameters.

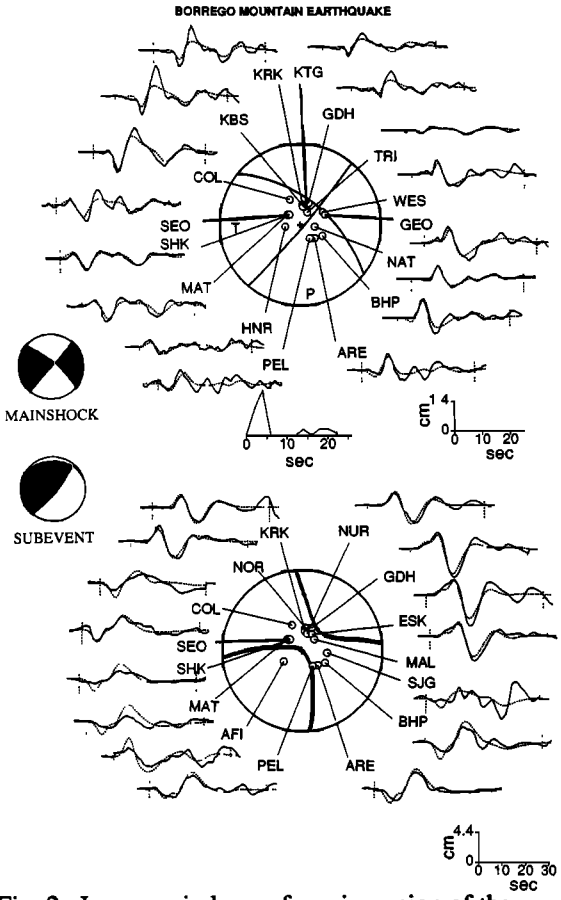

Fig. 2. Long-period waveform inversion of the 1968 Borrego Mountain earthquake. (Top) P waves and radiation pattern. (Bottom) SH waves and radiation pattern. Both observed waveforms (solid lines) and synthetics (dotted lines) are shown. The far-field source-time function is centered beneath P waveforms. Waveform scale for P waves is shown to right of source-time function and for SH waves at bottom right. Mechanisms of mainshock and subevent are shown to lower left of P waveforms on equal-area projections of lower hemisphere. Solid quadrants denote compressional P wave motion.

Our inversion results suggest a moment release in the second subevent of 2.6×10^{18} N m, nearly a third of the moment released in the first subevent. The mechanism for the second subevent indicates slip on either a shallow dipping thrust or a steep reverse fault striking northeast (Figure 2). The inversion results suggest a location for the second subevent well away from the master fault (about 25 km). The waveforms are best fit using a subevent located either northeast or southwest of the first subevent located on the Coyote Creek fault. These directions and distances correspond with two prominent aftershock clusters described by Das and Scholz [1981].

Burdick and Mellman [1976] also found energy release subsequent to the first subevent located on the Coyote Creek fault. They, however, separated the moment release into three subevents (instead of two). The second and third subevents from their inversion were located south of the first subevent. We used the source-time function of Burdick and Mellman [1976] and applied it to our data set to test the direction of our second subevent from the first subevent. We inverted for only two subevents, however, and not three subevents as in their inversion. Residuals were again minimized when moment in the subevents was released to either the northeast or southwest rather than from the south. Thus our inversion results indicate that a second subevent is located on a secondary fault to the northeast or southwest of the first subevent, located on the Coyote Creek fault.

Results of Waveform Inversion of the 1969 Earthquake

The waveforms of the 1969 Coyote Mountain event are much simpler but also noisier than waveforms of the Borrego Mountain event. We found that an inversion using a simple point source gives an adequate fit to the data and a result consistent with published short-period mechanisms

TABLE 1. Results of Inversions of Long-Period Data

Event	Strike, deg	Dip, deg	Slip, deg	Depth, km	Moment, x 10^{17} N m	Distance, km	Azimuth, deg
Borrego mainshock	311 ± 2	78 ± 2	179 ± 2	10 ± 1	92.0 ± 2.5	-	-
Borrego subevent	40 ± 7	80 ± 5	80 ± 10	7 ± 5	29.0 ± 5.0	25 ± 5	40 ± 10
Coyote Mountain	295 ± 5	69 ± 4	169 ± 4	12 ± 1	2.5 ± 0.7	-	-

[a] Standard errors of inversions from Nabelek [1984] are scaled similarly to those of McCaffrey [1989].

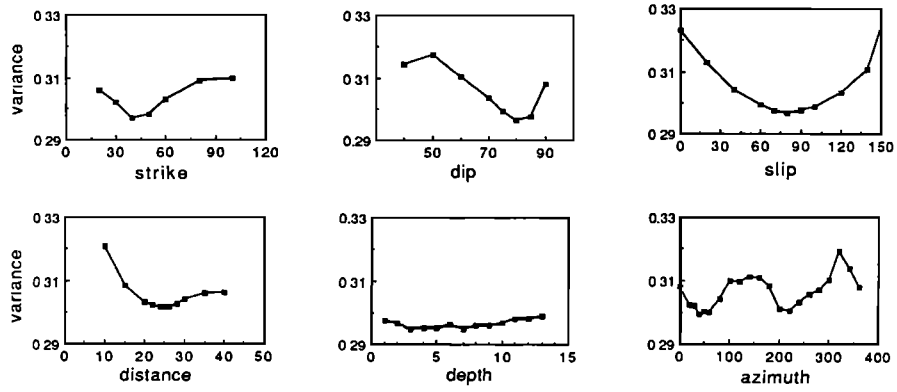

Fig. 3. Resolution of the second subevent parameters for the 1968 Borrego Mountain earthquake. While strike, dip, and slip show narrow well-defined minima, distance from centroid, depth, and azimuth of the subevent are poorly constrained.

[Thatcher and Hamilton, 1973]. The mechanism, waveforms, and source-time function from the Coyote Mountain inversion are shown in Figure 4 with parameters and uncertainties outlined in Table 1. The centroid depth is consistent with the 11 km depth for the mainshock inferred from the aftershocks [Thatcher and Hamilton, 1973].

A significant finding, however, is that the orientation of the northwesterly striking nodal plane of the Coyote Mountain event is inconsistent with the strike of the Coyote Creek fault. The latter strikes about 315° near the hypocenter, whereas a nodal plane with a strike of 295° allowed the best fit to the waveform data. We determined the resolution of the strike parameter in the inversion to interpret the 20° difference between the surface strike of the master fault and the orientation of the nodal plane. Error analysis of the second subevent indicates that strike parameters more than 10° from the 295° optimal value give residuals that are significantly higher at the 95% confidence level (Figure 5). Unless the strike of the fault changes significantly at depth, which we have no reason to believe, the 1969 event was probably not caused by rupture of the master fault. Regional cross faults strike about 40°, and our conjugate nodal plane strikes 29°, and dips 80° southeast, with a rake of 21°. Hence the strike of the conjugate nodal plane differs by about 11° from that of regional cross faults. This 11° discrepancy is within the error, considering that the inferred cross fault is not exposed. Aftershocks of the 1969 event span across the San Jacinto fault zone, between the two master faults, where several cross faults have been mapped. In addition, seismicity between 1981 and 1986 suggests that a cross fault is located near the 1969 aftershocks (discussed later). Thus a secondary fault rupture, probably a cross-fault rupture, may have caused the 1969 event rather than slip on a northwesterly striking master fault.

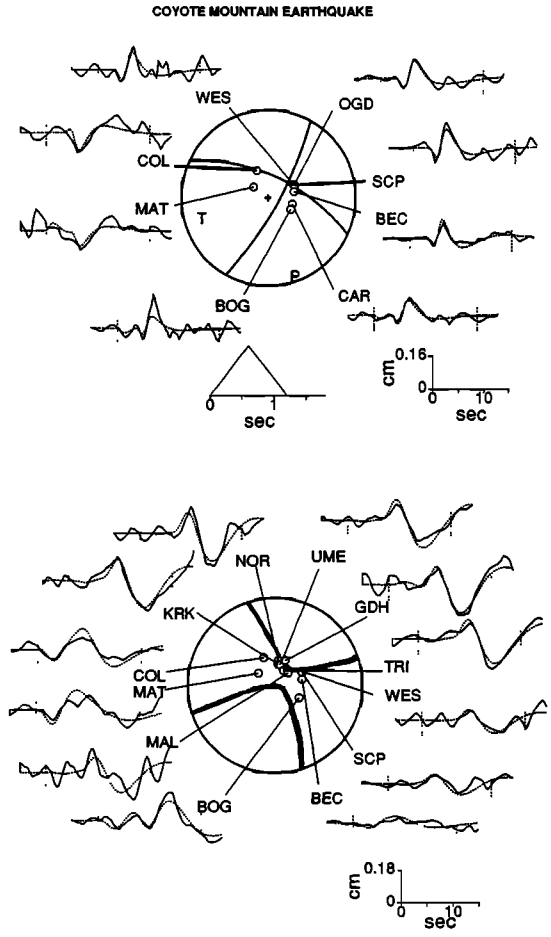

Fig. 4. Long-period waveform inversion of the 1969 Coyote Mountain earthquake. (Top) P waves and radiation pattern. (Bottom) SH waves and radiation pattern. Both observed waveforms (solid lines) and synthetics (dotted lines) are shown. The far-field source-time function is shown centered beneath the P waveforms. Waveform scale for the P waves is shown to right of source-time function and for SH waves at the bottom right.

SEISMICITY

The southern San Jacinto fault zone is one of the most seismically active regions of California (Figures

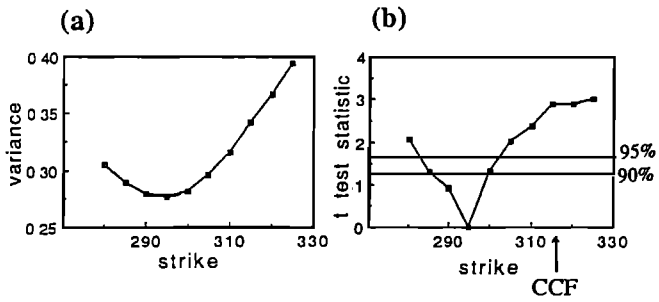

Fig. 5. Resolution of strike of the 1969 Coyote Mountain earthquake. (a) Variance exhibits a minima for strike parameter at 295°. (b) A t test indicates strike values that are significantly different at 90% and 95% confidence levels. All values of strike that have a t test statistic above one level, say 90%, have residuals that are higher than the minima at 90% confidence. The strike of the Coyote Creek fault is about 315° near the 1969 event.

6a and 6b) with earthquakes located on both master and secondary faults. While it has been long recognized that large deformations are accommodated by master faults, our research indicates that significant strain is also accommodated by cross faults. In the next section we investigate this hypothesis from the point of view of background seismicity. We choose to relocate earthquakes in a small area of the southern San Jacinto fault zone using a local velocity model. It is better to use these locations than simply use the catalog data that has been located with a regional velocity model. These relocated earthquakes allow us to study the detailed distribution and relationships of seismicity on both master and secondary faults.

Data and Relocation Procedure

While catalog hypocenters are useful in examining gross tectonic features, they are inadequate for local detailed tectonic analysis. Therefore we investigated recent fault activity by relocating travel time data from the California Institute of Technology / United States Geological Survey (CIT/ USGS) network collected between 1981 and 1986. Locations were obtained with HYPOINVERSE [Klein, 1978], downweighting stations greater than 50 km away from the epicenter. We relocated earthquakes using several regional velocity models [Hamilton, 1970; Fuis et al., 1982; Doser and Kanamori, 1986] and found that hypocenters using the Hamilton [1970] model were more tightly clustered and yielded the lowest travel time residuals. The Hamilton [1972] velocity structure was obtained from analysis of explosion data in the vicinity of the Borrego Mountain earthquake and appears to be a good approximation of the local velocities [Hamilton, 1970].

We unsuccessfully attempted to refine the Hamilton [1970] velocity model by inverting simultaneously for hypocenters and velocities using the method of Crosson [1976]. We inverted for events located on each side of the fault separately using only stations located on the same side of the fault as the earthquakes. For example, data from events located east of the fault were inverted using only stations on the east side of the fault. These inversions yielded different velocity models for each side of the fault.

To test whether these velocity models were significantly better than the Hamilton [1970] model, we relocated several hundred events using the new velocity models. While the residuals obtained using the new velocity models were lower than those obtained using the Hamilton [1970] model, residuals were significantly reduced only at the 60% confidence level. Results of many inversions indicate a velocity gradient, increasing about 10% from southeast to northwest. This result is consistent with mapped surficial geology, which indicates thick sediments on the east side of the Coyote Creek fault and crystalline rocks on the west side [Rogers, 1985], and heat flow data that indicates a northwest to southeast heat flow gradient [Doser and Kanamori, 1986]. The lithology may therefore be quite heterogeneous, and a three-dimensional inversion may be more appropriate than the method we applied.

Events recorded by a minimum of 15 stations were relocated using the Hamilton [1970] velocity model. The relocated hypocenters are compared with the same events from the southern California catalog (Figure 7). The structures are better delineated by the relocated hypocenters. Relocated seismicity allows features such as the Palm Wash fault to be distinguished from a simple cluster. Accurately relocated data from 1981 to 1986 are shown in Figure 6b. Histograms in Figure 8 indicate the vertical and horizontal standard errors of these relocated events. The standard errors of the depth (±2 km) and horizontal (±0.7 km) locations are small. Those uncertainties are smaller than the size of many features delineated by the seismicity. Therefore we suggest that these features are not simply artifacts of the relocation process; they reflect fault structure.

Seismicity Along the Palm Wash Fault

One of the most prominent features of the relocated seismicity from 1981 to 1986 is a cluster of earthquakes situated 25 km northeast of the Borrego Mountain epicenter (Figure 6c). This cluster is resolved into a narrow zone and is interpreted as a fault that has not been previously identified. This fault dips 70° to the east and strikes subparallel to the Coyote Creek fault (Figure 9a). The structure is named here the Palm Wash fault for a nearby topographic feature on the geologic map of California [Rogers, 1985]. Our best focal mechanisms from the relocated phase data indicate that right-lateral strike-slip faulting predominates on the Palm Wash fault.

The relocated seismicity on the Palm Wash fault correlates with a discontinuity in seismic reflectors observed on a reprocessed seismic reflection profile

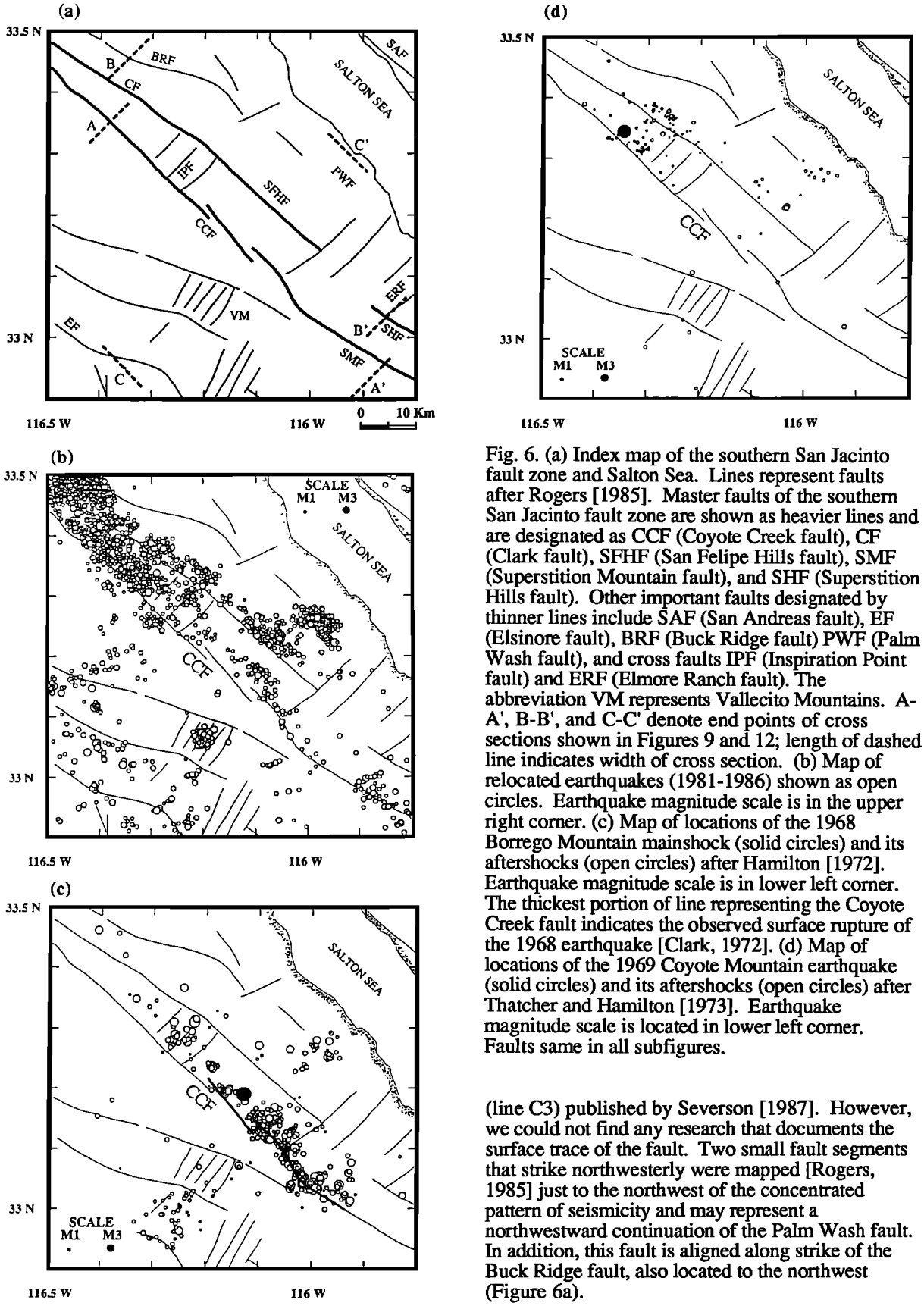

Fig. 6. (a) Index map of the southern San Jacinto fault zone and Salton Sea. Lines represent faults after Rogers [1985]. Master faults of the southern San Jacinto fault zone are shown as heavier lines and are designated as CCF (Coyote Creek fault), CF (Clark fault), SFHF (San Felipe Hills fault), SMF (Superstition Mountain fault), and SHF (Superstition Hills fault). Other important faults designated by thinner lines include SAF (San Andreas fault), EF (Elsinore fault), BRF (Buck Ridge fault) PWF (Palm Wash fault), and cross faults IPF (Inspiration Point fault) and ERF (Elmore Ranch fault). The abbreviation VM represents Vallecito Mountains. A-A', B-B', and C-C' denote end points of cross sections shown in Figures 9 and 12; length of dashed line indicates width of cross section. (b) Map of relocated earthquakes (1981-1986) shown as open circles. Earthquake magnitude scale is in the upper right corner. (c) Map of locations of the 1968 Borrego Mountain mainshock (solid circles) and its aftershocks (open circles) after Hamilton [1972]. Earthquake magnitude scale is in lower left corner. The thickest portion of line representing the Coyote Creek fault indicates the observed surface rupture of the 1968 earthquake [Clark, 1972]. (d) Map of locations of the 1969 Coyote Mountain earthquake (solid circles) and its aftershocks (open circles) after Thatcher and Hamilton [1973]. Earthquake magnitude scale is located in lower left corner. Faults same in all subfigures.

(line C3) published by Severson [1987]. However, we could not find any research that documents the surface trace of the fault. Two small fault segments that strike northwesterly were mapped [Rogers, 1985] just to the northwest of the concentrated pattern of seismicity and may represent a northwestward continuation of the Palm Wash fault. In addition, this fault is aligned along strike of the Buck Ridge fault, also located to the northwest (Figure 6a).

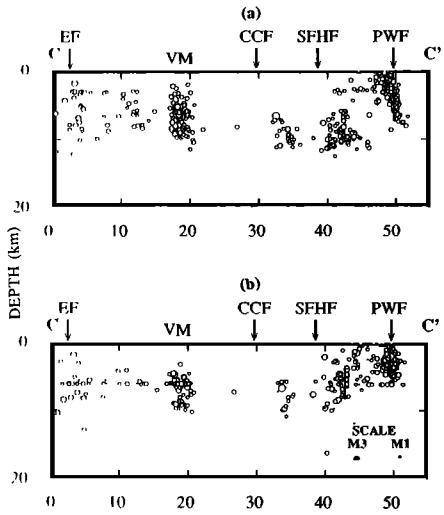

Fig. 7. Cross section C-C'. End points are shown in Figure 6. Horizontal distance is in kilometers. (a) Selected relocated earthquakes from 1981 to 1986 using Hamilton [1970] model. (b) Same earthquakes as in upper figure from the CIT/USGS catalog. Earthquake magnitude scale for both cross sections is in lower right corner.

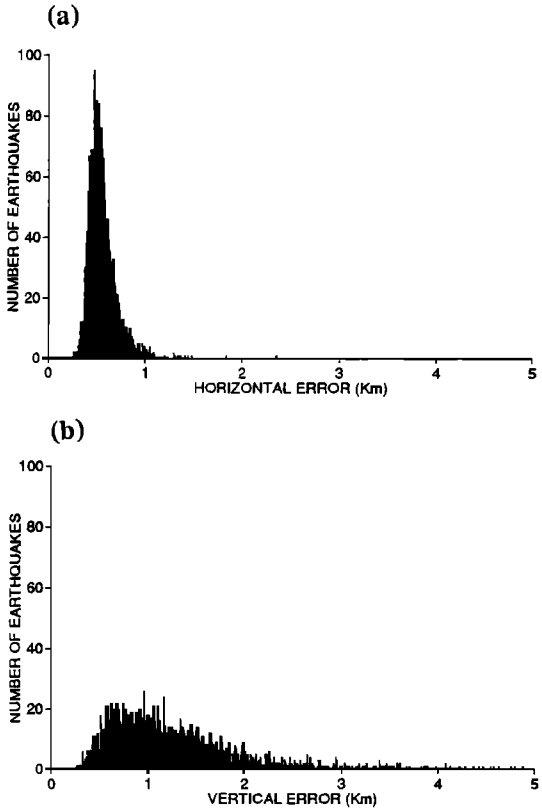

Fig. 8. Histograms showing projected (a) horizontal and (b) vertical standard errors (from HYPOINVERSE [Klein, 1978] of selected relocated data from 1981 to 1986 shown in Figures 6, 9, and 12.

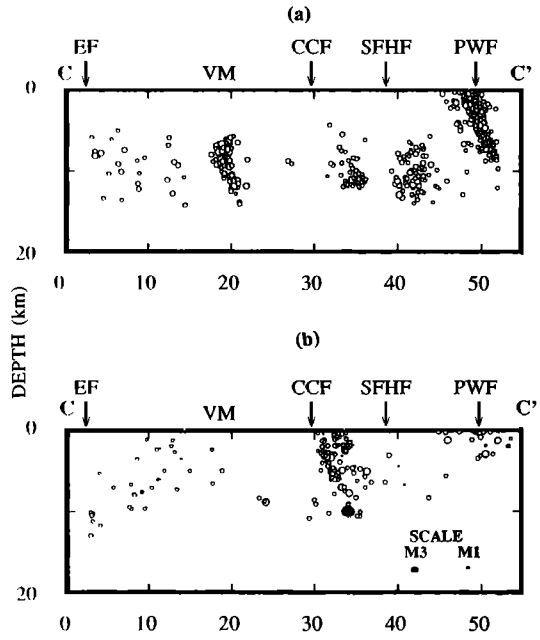

Fig. 9. Cross section C-C'. End points are shown in Figure 6. Horizontal distance is in kilometers. (a) Relocated earthquakes from 1981 to 1986 and (b) 1968 Borrego Mountain hypocenter (solid circle) and aftershocks (open circles). Both sections include events located within 5 km of cross section line in Figure 6a. Intersections of the Elsinore fault (EF), Vallecito Mountains (VM), Coyote Creek fault (CCF), San Felipe Hills fault (SFHF), and the Palm Wash fault (PWF) with cross section line are indicated as arrows above. Earthquake magnitude scale for both cross sections is in lower right corner.

Activity on the Palm Wash fault tends to be partitioned in space and time. During early 1981, just after the M_L=5.5 Westmorland earthquake, activity was high and concentrated over most of the southern Palm Wash fault. Between late 1981 to 1986, however, the rate of activity was much lower with most seismicity located north of the swarming activity in 1981. The activity to the south appears to have been largely shut off after the earthquake swarm in early 1981. The spatial distribution of the Palm Wash events suggests, however, that seismicity is confined to a single fault that strikes northwest.

We also observed a correlation between the timing of large regional events and the rate of seismicity on the Palm Wash and San Felipe Hills faults. Earthquake epicenters located within a 0.2° x 0.1° area between the Palm Wash and San Felipe Hills faults, were extracted from the CIT/USGS seismicity catalog. A histogram of the seismicity near the Palm Wash and San Felipe Hills faults (Figure 10a) shows the total number of events $M \geq 2.2$ recorded as a function of time. Histograms were produced for events $M \geq 2.2$, because we believe the catalog is complete at this magnitude level between 1979 and 1988 and is not biased by the station distribution. We found that significant peaks of activity begin in

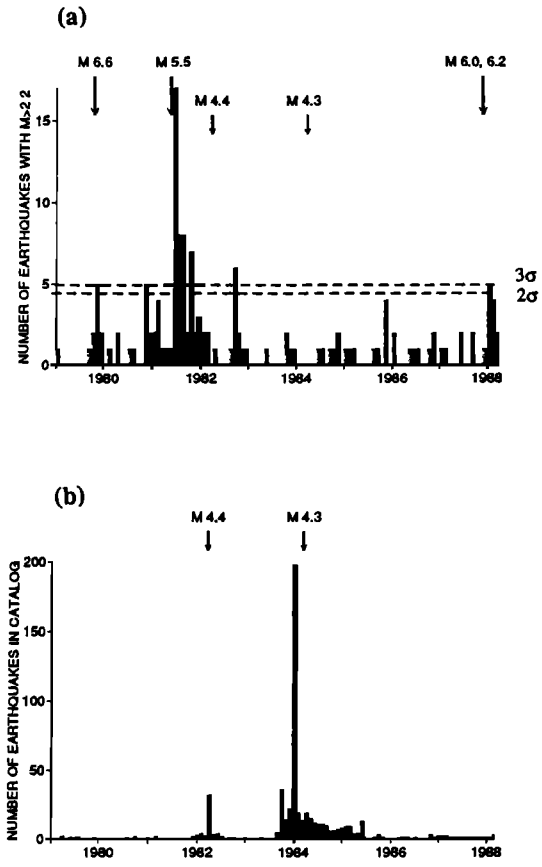

Fig. 10. Histograms showing number of earthquakes from the CIT/USGS catalog between 1979 and 1988 in an (a) 0.2° x 0.1° area located near the Palm Wash and San Felipe Hill faults and (b) 0.1° x 0.1° area located near the Vallecito Mountains. Arrows above histograms indicate dates of regional earthquakes with large arrows representing events of M5 to M6 and smaller arrows events M4 to M5. Dashed lines indicate two and three standard deviations from the average background seismicity and indicate peaks that are significantly different than the average seismicity.

November 1979, November 1980, June 1981, September 1982, and January 1988 (Figure 10a). These peaks are significantly higher than the background seismicity by two standard deviations when using all the data or three standard deviations when eliminating the highest peak in 1981 (Figure 10a). We calculate an average rate of 1.2 events per month over the 10 year time period for events with M ≥ 2.2.

Regional events of M > 4 were also extracted from the catalog with the following criteria: 4 < M < 5 events within a circle of 30 km radius, 5 < M < 6 events within a circle of 40 km, and M > 6 events within a 60 km radius from the center of the Palm Wash fault. Three regional earthquakes of M > 5 fit the distance criteria described in the time interval between 1979 and 1988: the October 15, 1979, Imperial Valley (M_L=6.6), the April 28, 1981, Westmorland (M_L=5.5), and the November 24, 1987, Elmore Ranch and Superstition Hills events (M_L=6.2 and 6.6). Because the two earthquakes in 1987 occurred so close in time and are related tectonically, we consider these events as a single sequence for the purpose of correlation with changes in the level of seismicity.

The rate of seismicity recorded near the Palm Wash and San Felipe Hills faults correlates well with the occurrence of large (M ≥ 5.5) regional events (Figure 10a). Each of the three regional earthquake sequences is followed within two months by a significant peak of activity. Given that we have a 107 month sample, the probability of having one earthquake occur randomly two months prior to the one of the five significant peaks of activity would be 10/107. Therefore the joint probability that the three regional earthquakes would randomly occur prior to the five significant peaks is even lower, less than 1%. Thus we conclude that this correlation between large regional earthquakes and an increased period of seismicity near the Palm Wash and San Felipe Hills faults is significant.

Two of the five significant peaks in the local seismicity are, however, not correlated with large regional moment release. Moreover, the M=4.4 and M=4.3 events in Figure 10a also do not appear to increase the seismicity (M ≥ 2.2) on the Palm Wash or San Felipe Hills faults. A peak of activity on the Palm Wash and San Felipe Hills faults typically begins several days to a month following each regional event (M > 5.5) and persists for up to five months. Thus we suggest that the increased rate of activity on the Palm Wash and San Felipe Hills faults following regional events is not coincidental but is reflecting either the interaction between faults or regional stress changes.

Seismicity Beneath the Vallecito Mountains

An intense burst of seismicity (Figure 6b) occurred in late 1983 beneath the Vallecito Mountains (VM in Figure 6a). Relocated hypocenters of this swarm define a zone that is narrow horizontally but stretches about 10 km in depth, primarily between 5 and 15 km (Figure 9a). This seismicity is centered near the intersection of mapped northeast trending cross faults and northwest trending faults that are oriented subparallel to the master faults (Figure 6a). Focal mechanisms that we produced indicate a prevalence of strike-slip motion on planes parallel to either the cross faults or the northwest trending faults. Stress concentration at the intersection of the cross faults and northwest trending faults may account for this tight cluster and for its vertical elongation.

The Vallecito Mountain cluster became active prior to nearby large or moderate events on the Coyote Creek fault and may therefore be a useful short- or intermediate-term precursor to large earthquakes in this area. A histogram (Figure 10b) indicates the rate of seismicity as a function of time in a 0.1° x 0.1° area centered over the Vallecito Mountain cluster. About 200 events were recorded in one month

beneath the Vallecito Mountains; none of these had M > 4 (Figure 10b). Nearly a month following the Vallecito Mountain earthquake swarm, a M_L=4.3 event occurred near the Coyote Creek fault. This event was the only M > 4 event to occur near the Coyote Creek fault between 1981 and 1986 (Figure 11). The proximity and timing of the swarm and the Coyote Creek event indicate that these events may be related. The M_L=4.4 event of 1982 in Figure 10b was the largest event in that smaller swarm. That swarm does not appear to be related to a M > 4 event outside of the swarm area.

A burst of earthquake activity was also reported beneath the Vallecito Mountains prior to the 1968 event (Figure 11) [Sanders and Kanamori, 1984]. Thus two periods of increased seismicity preceded moderate to large events on the master Coyote Creek fault. This activity may be related to cross fault interaction with the master fault, or it may simply be related to a regional change in mechanical conditions such as stress or fluid pressure. However, one must be careful about drawing conclusions about seismic precursors from seismicity that spans only a short time.

Seismicity Along the Coyote Creek Fault

Seismicity along the master fault strand that ruptured in 1968 is currently low above 8 km depth and indicates that most of the fault is locked (Figure 12b). Only one of our relocated events with M > 4

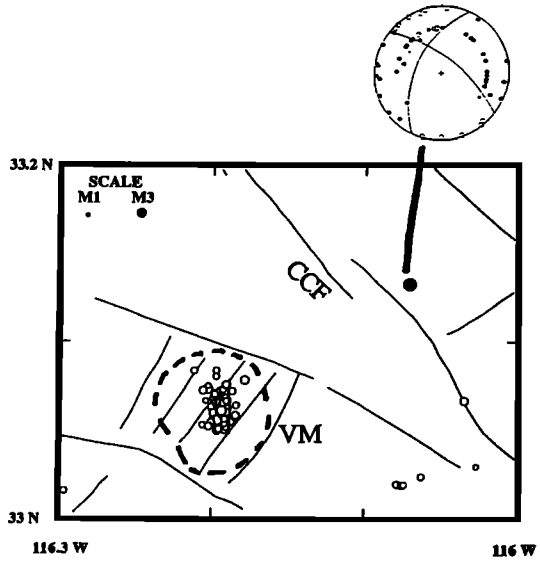

Fig. 11. Map of Coyote Creek fault (CCF) and Vallecito Mountain area (VM) showing the relationship of the swarm in December 1983 and the M=4.3 event in February 1984 on the Coyote Creek fault (solid circle). Dashed line indicates locations of preshocks to the 1968 event [Sanders and Kanamori, 1984]. Inset shows first motion focal mechanism of the 1984 event. Magnitude scale is in upper left corner of map. Faults are same as Figure 6.

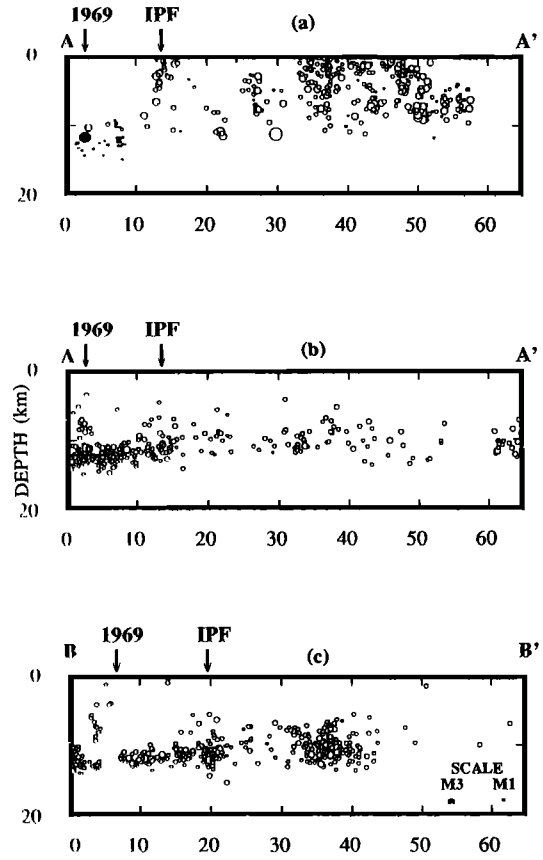

Fig. 12. Cross section A-A' and B-B'. End points are shown in Figure 6. Horizontal distance is in kilometers. Sections include events 5 km from cross section line. Arrows designate probable intersection of cross faults. (a) Cross section A-A'. 1968 mainshock and aftershocks (open circles) and the 1969 mainshock and aftershock (solid circles). Left arrow indicates location of inferred cross fault active in the 1969 event; right arrow shows location of the mapped Inspiration Point fault (IPF) that became active following the 1968 event. (b) Cross section A-A'. Relocated earthquakes from 1981 to 1986 near the Coyote Creek fault. Arrows are same as in Figure 12a. (c) Cross section B-B'. Relocated earthquakes from 1981 to 1986 near the Clark and San Felipe Hills faults. Earthquake magnitude scale for all cross sections is in the lower right corner.

was most likely located on the Coyote Creek fault (M_L=4.3 in February 1984; see Figure 11). Unlike the Palm Wash and San Felipe Hills faults, the Coyote Creek fault does not appear to be stimulated by regional stress release. The 1984 event was located about 10 km southeast of the 1968 hypocenter and was preceded by activity beneath the Vallecito Mountains (described above). The focal mechanism we obtained for the event suggests right-lateral strike-slip motion, with a large component of normal faulting down to the east on the plane parallel to the Coyote Creek fault (Figure 11). This normal faulting component of the earthquake mechanism

may be related to the nearby extensional jog in the Coyote Creek fault.

Although the 1984 M_L=4.3 event occurred at a depth of only 6 km, background activity near the Coyote Creek fault is primarily restricted to depths between 8 and 10 km near the 1968 epicenter and below 10 km to the northwest of that earthquake (Figures 12a and 12b). In fact, this background seismicity becomes 2 to 4 km deeper from south to north, plunging about 3° to the north. The few events from 1981 to 1986 that appear to be located on the master fault are clustered and do not clearly delineate the fault as did aftershocks of the 1968 event. Indeed, the seismicity from 1981 to 1986 is not located where aftershocks of the 1968 event occurred but instead defines a ring about the aftershock zone (Figures 12a and 12b).

Abundant microseismicity may indicate portions of the fault that do not rupture in large earthquakes, and areas that lack this background seismicity may indicate regions that are capable of rupture in large events. This pattern was observed in the Loma Prieta segment of the San Andreas fault [Plafker and Galloway, 1989] and along the Calaveras fault [Oppenheimer, et al., 1990]. While Louie et al. [1985] note, however, that the Coyote Creek fault may be creeping aseismically at the surface, we agree with Hudnut and Clark [1989] that this creep is continued afterslip of the 1968 event and involves only the uppermost kilometer of sediments. Therefore the seismicity rate and pattern indicate that the segment of the Coyote Creek fault that ruptured in 1968 is currently locked and building up stress.

Seismicity Along the Clark and San Felipe Hills Faults

The relocated seismicity is concentrated along the northwestern portion of the San Jacinto fault zone from 1981 to 1986. This seismicity is scattered between the master strands (Figure 6b). The seismicity occurs below 10 km (Figure 12c) and deepens to the north, similar to that observed along the Coyote Creek fault (Figure 12b). In fact, seismicity above 10 km tends to occur on cross faults. A cross section B-B' (Figures 12b and 12c) indicates that two cross faults were active from 1981 to 1986 between the San Jacinto master faults. Thus much of the interseismic activity may occur on either cross faults located between the two master strands or below 10 km on the master fault. The sections of these master faults that lack seismicity above 10 km probably are locked.

Seismicity on the southern San Felipe Hills fault appears to correlate with large regional moment release, similar to activity on the adjacent Palm Wash fault (described above). Events in 1979, 1981, and 1987 induced activity on the section of the fault that ruptured in the 1954 earthquake as defined by Sanders et al. [1986]. In this portion of the San Felipe Hills fault (between 30 and 45 km in Figure 12c), naturally induced seismicity is located in a cluster between depths of 5 and 13 km. Residual stresses that were not released during the 1954 event may be slowly released by large regional events.

Seismicity on Cross Faults

Combined and separate SPOT and Landsat images indicate that northeasterly striking cross faults are a more prominent feature of this region than has previously been appreciated [Rockwell, et al., 1990]. Many of these cross faults are seismically active and some are known to have ruptured in large events. Probably the best documented example of cross-fault activity in southern California is the 1987 rupture on the Elmore Ranch fault [Hudnut et al., 1989b]. Doser [1990] completed a body waveform inversion of the 1942 earthquake and its largest aftershock and concluded that these events may also have occurred on northeast trending cross faults (Figure 1).

The relocated seismicity indicates that cross faults are active, especially in the southern part of the San Jacinto fault zone. Close observation of the relocated seismicity in this zone reveals that many events are aligned along northeast trends. Cross sections A-A' (along the Coyote Creek fault) and B-B' (along the Clark and San Felipe Hills faults) indicate intersections of two cross faults and the master faults (Figures 12b and 12c). Arrows above cross sections in Figure 12 indicate the locations of intersections of both the cross fault that may have caused the 1969 rupture and the Inspiration Point fault that ruptured in conjunction with the 1968 event. Seismicity above 10 km depth is aligned along a cross fault (see left arrow marked 1969 on Figure 12) that may have caused the 1969 event. In addition the mapped Inspiration Point fault (see right arrow marked IPF on Figure 12) appears to have been active between 1981 and 1986, although this activity is not as clearly aligned along a single fault. Thus much of the recent seismicity above 10 km occurs on cross faults.

1968 and 1969 Aftershocks

The 1968 aftershocks located by Hamilton [1972] and the 1969 aftershocks located by Thatcher and Hamilton [1973] indicate rupture not only on master faults but also on several secondary faults: the Palm Wash fault, the Inspiration Point fault, and faults located near the Vallecito Mountains (Figure 6a, 6c, and 6d). Das and Scholz [1981] proposed that the stress field associated with the occurrence of the 1968 event could induce the observed aftershocks on the Palm Wash fault and near the Vallecito Mountains.

Aftershocks of the 1968 event delineate the structure of the Coyote Creek fault. These events trend about 315°, consistent with surface rupture [Clark, 1972], and dip about 85° to the northeast (Figure 9). Earthquakes extended from the mainshock at a depth of about 10 km up to the surface. Aftershocks near the northern end of the 1968 rupture trend northeast and are located near a mapped cross fault, the Inspiration Point fault (Figures 6a and 6c). The few earthquakes located

north of this cross fault (cross section A-A', Figure 12a) were deeper than events located to the south. The Inspiration Point fault that was active at the northern end of the 1968 rupture zone may have created a barrier that controlled the extent of that rupture [Seeber and Nicholson, 1986].

Our inversion results for the 1969 earthquake indicate that the master fault is significantly misoriented with respect to the northwest nodal plane of the focal mechanism. Thus the event was probably caused instead by rupture along a northeast cross fault. The 1969 aftershocks were significantly deeper than the 1968 sequence [Thatcher and Hamilton, 1973] and occurred primarily north of the Inspiration Point fault that may have controlled the rupture in 1968 (Figures 6d and 12a). These aftershocks were scattered between the two master faults (Figure 6d), similar to the pattern of recent earthquakes located in the same area (Figure 6b). Thus the 1969 rupture appears to have involved slip on a cross fault, perhaps as static fatigue following the 1968 shock reduced the strength of its barrier or asperity.

SEISMIC HAZARD

Potential of Cross Faults to Generate Significant Earthquakes

Many cross faults are mapped west of the Salton Sea (Figure 6a). Several cross faults are mapped between the two master strands of the San Jacinto fault zone; other cross faults are known outside of this fault zone. Seismicity has been associated with many of these cross faults. Cross faults could rupture in large earthquakes, and those events could trigger earthquakes on adjacent master faults, similar to the 1987 sequence. Some large earthquakes occurred on previously unrecognized cross faults. The Elmore Ranch fault that ruptured in 1987 (Figure 6a) and the cross fault that ruptured during the 1981 Westmorland earthquake are examples of such faults. Many other as yet unmapped cross faults may be capable of producing significant earthquakes.

Several cross faults could rupture in $M > 5$ earthquakes. Hudnut et al. [1989a] suggest that the Extra fault, a cross fault that is located between the San Andreas and San Jacinto faults, could itself rupture in a large event or could trigger the occurrence of large events on one of the nearby master faults. Other cross faults with seismic potential are located near the Vallecito Mountains, just north of the Elmore Ranch fault, and between the master faults (Figure 6a). These cross faults can rupture in moderate to large events and should be considered in seismic hazard evaluations.

Seismic Gaps Along Master Fault Strands

Two types of seismic gaps are situated along the southern San Jacinto fault zone. We observe patterns of seismicity and quiescence between 1981 and 1986 that allow definition of these seismic gaps. The first type of gap is characterized by fault segments that have not ruptured in historic earthquakes but have abundant microseismicity near a depth of 10 km and minimal seismicity above a depth of 10 km. The second type of gap includes segments that have low microseismicity throughout the seismogenic zone. Both types of gaps are located on or between mapped faults and have adjacent segments that have ruptured in historic large events.

The first type of gap occurs along master faults located northwest of the 1968 rupture zone. The Coyote Creek, San Felipe Hills, and Clark faults (Figure 6a) all exhibit this type of seismic behavior. Recent seismicity between 1981 and 1986, interseismic activity, is abundant along master faults (Figure 6b). Most of this seismicity is, however, located at or below about 10 km depth (Figures 12b and 12c); the upper 10 km is primarily quiescent. Since we know that a large earthquake occurred in 1968 along the Coyote Creek fault and ruptured mostly above a depth of 10 km, we can infer that large earthquakes may rupture the fault above the deep characteristic interseismic activity. Hence those portions of the master fault that are quiescent during interseismic periods may be capable of breaking in large earthquakes even though there may be abundant seismicity at depth. Using this analogy we identify two segments along the Coyote Creek and Clark faults that may be capable of rupturing in large events. These gaps are shown as dashed lines in Figure 1.

We suggest that the 1969 event was deep and may have even ruptured along a cross fault. Therefore a gap along the Coyote Creek fault would extend from the northern end of the 1968 rupture to the intersection of the Coyote Creek and Clark faults (Figure 1). This gap would include much of the southern portion of the Anza gap as originally defined by Thatcher et al. [1975] (Figure 1). The gap along the Clark fault is not as clearly defined. The gap extends south to the 1954 rupture but may extend as far north as the 1980 (M_L=5.5) rupture or possibly even through the Anza gap (Figure 1) [Sanders et al., 1986]. The size of this gap depends on whether or not the 1937 and 1980 earthquakes released stress on the Buck Ridge, Clark, or cross faults. We have shown a conservative gap estimate in Figure 1 assuming that the 1937 event occurred on the Clark fault.

Seismic quiescence defines our second type of seismic gap and occurs along master faults located primarily south of the 1968 rupture zone. Although northwest trending master faults are mapped, minimal microseismicity occurs along these segments. The Superstition Hills, Superstition Mountain faults, and the area between the Superstition Hills and San Felipe Hills faults are examples of segments that exhibit this type of seismic behavior. The Buck Ridge fault (located north of the 1968 rupture) also exhibits low seismicity between 1981 and 1986. These quiescent faults are, however, known to be capable of producing large earthquakes (e.g., the 1987 Superstition Hills event). Thus such quiescent

regions that are aligned along northwest trending faults or along strike of these faults may have considerable seismic hazard. We identify one gap located between the 1954 and 1987 rupture zones that may be capable of generating a large earthquake (Figure 1).

FOCAL MECHANISMS AND TECTONICS

We compute focal mechanisms for many earthquakes in the southern San Jacinto fault zone and adjacent faults. These mechanisms allow us to study the detailed kinematics of earthquakes on the master and secondary faults. The abundance of short-period phase data from the CIT/USGS network allows many fault plane solutions to be produced, revealing details of faulting. Seeber and Armbruster [1988] developed a grid search method for computing first-motion focal mechanisms. We computed several hundred focal mechanisms for the earthquakes located with the Hamilton [1970] velocity model. To obtain the best possible mechanisms, only those events that were deeper than 5 km and possessed greater than 10 weighted arrivals were considered. Many of these computed mechanisms were rejected due to inconsistencies in polarities within focal quadrants.

While a few of the individual solutions may be poorly constrained, the majority of the solutions allow only small changes in the orientation of focal planes. Moreover, the large quantity of solutions permits a statistical analysis of the results. Not only were earthquake phase data from the relocated events computed using the grid search algorithm, many were also checked visually. The grid search method gave results similar to analysis of individual events.

The compressional (P) and tensional (T) axes of the solutions are separately plotted in Figure 13 to show regions where each of the different fault styles may be active. The region west of the Salton Sea appears to be structurally complex, with events having strike-slip, thrust, and normal-faulting mechanisms. Most of the mechanisms suggest large strike-slip components of motion; P and T axes are nearly horizontal (Figure 13). Solutions for events on the Coyote Creek, San Felipe Hills, Palm Wash, and Elsinore faults as well as beneath the Vallecito Mountains all have large strike-slip components.

Normal faulting is suggested by mechanisms of events in a small cluster just 10 km southeast of the Vallecito Mountains (see steeply dipping P axes indicated by short-line segments in Figure 13). Many mechanisms are predominantly strike slip but involve sizable components of thrust or normal faulting motion. The Salton Trough is an extensional basin, and normal mechanisms would be expected. In fact, a simple extensional tectonic framework would predict more normal fault mechanisms than were observed in the data. Compressional and tensional axes are plotted in Figure 14 and indicate that more P axes than T axes are vertical. This result suggests a predominance of normal faulting with respect to thrust faulting. We also obtain only a few mechanisms that include nodal planes that suggest detachment faulting.

All compressional and tensional axes are consistent with a single stress field oriented about north-south (Figure 14). This result is consistent with north-south regional stress indicators [Jones, 1988; Sanders, 1990]. The hemisphere projection can be

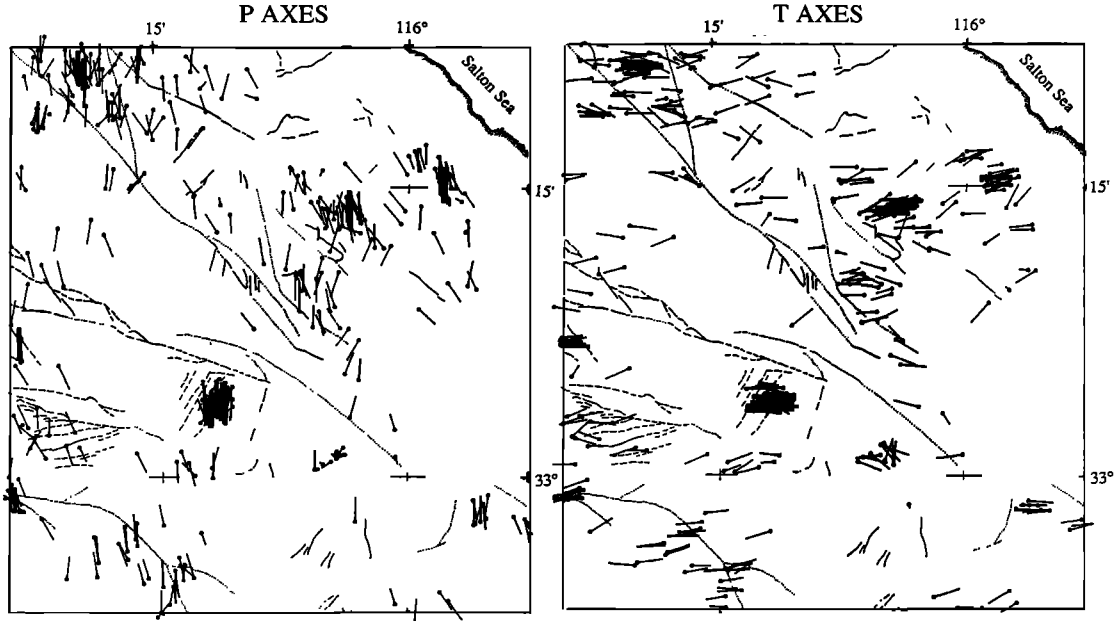

Fig. 13. Map of southern San Jacinto fault zone with faults (dotted lines) after Rogers [1985]. Compressional axes (P axes, left figure) and tensional axes (T axes, right figure) are from mechanisms determined in this study. Length of line is proportional to cosine of dip; i.e., horizontal dip has a longer length, and near vertical has a shorter length.

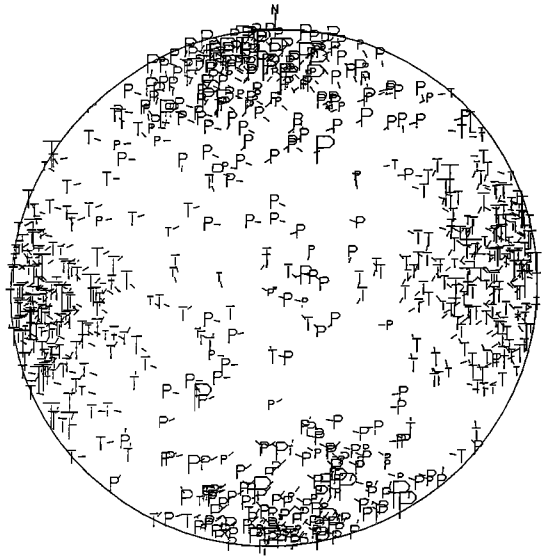

Fig. 14. P and T axes of events in Figure 13 projected on upper hemisphere equal-area projection. Dash mark next to each P axis indicates direction to T axis located 90° away and vise versa.

neatly separated into four quadrants with P and T axes distributed throughout each of the quadrants. Since much of the relocated seismicity occurs on secondary faults, we assume that our mechanisms are from earthquakes located on a wide orientation of faults and not simply from events located along the San Jacinto master faults. Thus the P and T orientations on this plot are taken to be indicative of an average regional stress with maximum compression oriented about north-south and least compression oriented about east-west.

Even though the orientations of P and T axes are locally consistent, compressional axes of earthquakes located in the Vallecito Mountain cluster differ from axes of events situated on the Palm Wash fault (Figure 13). Events located beneath the Vallecito Mountain have P axes with a mean trend of 7° azimuth and 8° plunge, whereas P axes of events situated on the Palm Wash fault have a mean azimuth of 352° and a plunge of 5°. The null hypothesis of sameness of the two populations can be rejected at the 98% level by Fisher statistics [Fisher, 1953; McFadden and Lowes, 1981]. Thus axes from events located on the Palm Wash fault are rotated with respect to those beneath the Vallecito Mountains. The events in these two clusters must have occurred on faults that differ significantly in orientation. Perhaps many of the events beneath the Vallecito Mountains are rupturing along cross faults that have been mapped in the area. Alternatively, unusual fluid pressures may be present at that cluster that lead to different effective (intergranular) stresses.

DISCUSSION

Fault activity to the west of the Salton Sea involves complex dynamics and coupling between faults. Major bursts of earthquakes were observed along secondary faults both prior to and after moderate to large regional events. Earthquake swarms were observed between 2 years and a few months prior to the 1937, 1954, and 1968 events [Sanders and Kanamori, 1984; Sanders et al., 1986]. Activity beneath the Vallecito Mountains also occurred prior to the 1968 and 1984 events. These small earthquakes may be acting as a kind of meter signaling a rise in stresses, similar to a persistent source of swarms located near the Anza gap, the so-called Cahuilla swarm [Sanders and Kanamori, 1984]. Seismic moment release has been found to increase over a wide area prior to large earthquakes in northern California [Sykes and Jaumé, 1990]. Hence forerunning activity occurs not only on one fault, but over a large region. An earthquake swarm such as that near the Vallecito Mountains may simply be responding to a regional stress increase.

Mechanisms for the interaction that leads to concentrations of stress in both space and time may involve cross faults, detachments, or pore fluid diffusion. Large earthquakes may induce seismicity on faults located at considerable distance (Figure 10a). The Palm Wash and San Felipe Hills faults are located about two rupture lengths away from both the 1979 and 1981 rupture zones. However we found a temporal relationship between the 1979 rupture and activity located about 60 km north on the Palm Wash and San Felipe Hills faults.

Four mechanisms have been proposed to explain load transfer that may induce seismicity on the Palm Wash and San Felipe Hills faults. One mechanism suggests that static strain or stress changes from an earthquake can induce seismicity on other nearby faults (Das and Scholz, 1981). A second mechanism implies that strain may propagate in the viscoelastic layer of the crust by spatial diffusion [Knopoff, 1989]. In a third mechanism, detachment faults may transmit strain by elastic creep (G.C. Bond et al., unpublished manuscript, 1990). In a fourth mechanism, increased pore fluid pressures can lower the effective stress on the fault and promote failure [Simpson, et al., 1988; Hudnut et al., 1989a].

Static strain changes associated with regional energy release are capable of inducing seismicity on nearby faults. We tested whether or not static strain changes from the 1979 Imperial Valley earthquake would be sufficient to induce activity near the Palm Wash or San Felipe Hills faults located about 60 km north of that rupture. The 1979 event was modeled with a 1 m dislocation 12 km wide and 33 km long [Savage, 1980]. The static strain changes near the Palm Wash fault resulting from this dislocation are of tidal order (1 to 2 x 10^{-7}). Thus the 1979 earthquake could probably not induce activity in the distance range of the Palm Wash fault from simple static strain changes. It also seems unlikely that these strains could cause significant changes in fluid pressures at that distance and thereby change the effective stress on faults. Thus mechanisms for spatial diffusion of pore fluids or static strain caused by a large regional event do not appear to be viable

mechanisms for inducing the observed rise in seismicity at the Palm Wash or the San Felipe Hills faults.

Strain relaxation in a midcrustal viscous layer is another mechanism that may induce seismicity. Knopoff [1989] suggests that stresses beneath a fracture are redistributed by local relaxation and by spatial diffusion in the subseismogenic layer. This mechanism has the advantage of explaining a time delay between the regional event and the induced seismicity. We modeled the time delay observed from the seismicity by calculating the relaxation time for a Maxwell viscoelastic material. Using upper and lower bounds of 10^{18}-10^{20} Pa s for viscosity of the uppermost asthenosphere inferred from glacial rebound [Walcott, 1973] and 4-7 x 10^{10} Pa for Young's modulus inferred for characteristic asthenosphere lithology [Turcotte and Schubert, 1982] we obtain a minimum viscoelastic relaxation time of about 1 year. Thus, unless the viscosity is significantly lower than the value that we used, the relaxation time is much longer than the month time delay that we observe. Therefore we would not expect a viscoelastic diffusion mechanism to have propagated the load over a 60 km distance in such a short time.

Another mechanism that could induce regional activity is slip along a subhorizontal detachment fault. The second subevent of the 1968 earthquake waveform inversion had a nodal plane that was consistent with either a subvertical or detachment fault. It released nearly a third of the moment of the first subevent on the Coyote Creek fault. The location of this subevent is poorly constrained and therefore difficult to associate with a specific fault. The nodal plane that corresponds with the fault that ruptured in the second subevent is not clear from the waveform inversion.

The source duration and magnitude determinations suggest, however, that a detachment fault may have ruptured in the 1968 earthquake. The subevent ruptured rather slowly over a 12 s duration (see source time function, Figure 2). Such a slow rupture may be more characteristic of detachment than reverse faulting. We estimate a moment magnitude, including both the first and second subevents, of 6.6 from our body wave inversion of the 1968 event. This magnitude is consistent with a body wave magnitude (Mb) of 6.6 but it is quite different from the surface wave magnitude (Ms) of 7.0; both these values were reported by Abe [1981]. Perhaps long-period energy was radiated slowly from a detachment fault, causing the long-period surface waves to be relatively larger than the short-period body waves. This slow radiation, rich in long-period energy, is consistent with rupture along a detachment fault. Detachment faults are not observed to be seismically active and are therefore often inferred to move aseismically.

The Borrego area is characterized by east dipping Miocene detachments and a metamorphic core complex [Blom et al., 1988; Engel and Schultejann, 1984]. G.C. Bond et al. (unpublished manuscript, 1990) suggested from geological and geophysical data that the Salton Trough basin may have been formed by a simple shear (detachment) mechanism rather than by pure shear, the more commonly assumed process. If they are correct, the inferred southeast dipping detachment fault system probably extended into the Palm Wash area and could have been reactivated during the 1968 event. Detachments are also an important element for block rotation, such as that inferred from paleomagnetic data near the Inspiration Point fault [Scheuing and Seeber, 1989]. Only a few mechanisms that had a nodal plane consistent with detachment faulting were computed in our study. However, Nicholson et al. (1986) found focal mechanisms that were consistent with detachment faulting to the north in the Transverse Ranges. In addition, P.A. Cowie and L. Seeber (unpublished manuscript, 1991) use gravity data to model a normal component of faulting on the cross faults. From this data, they model a detachment system that extends through the Borrego area, probably below the seismogenic zone. Thus we prefer a detachment mechanism for generating induced activity on the Palm Wash and San Felipe Hills faults at relatively great distances from large regional events.

CONCLUSIONS

Seismicity patterns, waveform inversions, and focal mechanisms indicate that many recent earthquakes in and near the San Jacinto fault zone occurred on secondary faults. The waveform inversion of the 1969 event and aftershocks of the 1968 and 1969 events indicate that northeast striking cross faults are active west of the Salton Sea. Two cross faults were recently active in the northwest San Jacinto fault zone: the Inspiration Point fault that was also active in conjunction with the 1968 event and the other that was most likely active during the 1969 earthquake. Such cross faults may control the characteristic length of the rupture on a master fault (e.g., the 1968 earthquake); they may also trigger events on a master fault (e.g., the 1987 events). Thus cross faults may be an important component of the rupture process of large events along master faults.

Secondary faults are also capable of producing earthquakes of large seismic moment. Our waveform analysis of the second subevent of the 1968 event indicates that slip along a reverse or detachment fault radiated nearly a third of the total moment of the Borrego Mountain event. The 1969 event (M_L=5.8) may have ruptured a northeast trending left-lateral cross fault rather than a northwest striking master fault. Our evidence for this hypothesis is first, the statistically significant mislocation of the nodal plane in our waveform inversion with respect to the master fault orientation. Second, the aftershock pattern is scattered and not simply located on the master fault. Third, recent cross fault ruptures in the region (e.g., the 1987

earthquakes) indicate that one cannot assume (a priori) that a rupture near the master fault is located on that fault. Secondary faults are important in seismic hazard assessment in this region.

We used the velocity model of Hamilton [1970] to relocate seismicity between 1981 and 1986 in the study area. This model appears to be a good approximation of the velocity structure near Borrego Mountain. The relocated seismicity allows finer resolution of structures than is possible using catalog locations. We named and characterized seismogenetically the Palm Wash fault that strikes northwest subparallel to the master faults, dips 70° to the east, and slips right laterally. Regional moderate to large events were correlated with significant peaks of activity on the Palm Wash and San Felipe Hills faults. We also characterized a cluster of earthquakes beneath the Vallecito Mountains that occurred in late 1983. The earthquake swarm occurred one month prior to a moderate size event on the Coyote Creek fault. This same area was also active prior to the 1968 earthquake. Thus the swarm beneath the Vallecito Mountains may be a short- to intermediate-term precursor to activity on the Coyote Creek fault.

Recent seismicity (1981-1986) that occurs on the Coyote Creek fault is distributed around the aftershocks of the 1968 event. Current background seismicity associated with the Coyote Creek, Clark, and San Felipe Hills faults deepens to the north and is primarily located deeper than 10 km. This characteristic deep seismicity below 10 km and lack of seismicity at shallower depths most likely indicate that the master faults are presently locked above 10 km and are currently building up stress. Comparison of the 1968 aftershock sequence and recent seismicity indicate that activity beneath 10 km depth occurs during the interseismic period and that large earthquakes rupture the fault above that level. Using this analogy with other portions of nearby master faults, we find that seismic gaps are located along the northwest Coyote Creek fault as well as along two segments of the Clark and San Felipe Hills faults. Several identified cross faults as well as many unidentified faults may also rupture in large earthquakes.

Compressional and tensional axes from mechanisms of events located west of the Salton Sea indicate a predominance of strike-slip motion and a north-south orientation of the average regional maximum compressive stress. This motion is consistent with transverse motion between the Pacific and North American plates. Although the location of the study area within the Salton Trough would also imply a large amount of extension, only one cluster of events located just outside the San Jacinto fault zone has mechanisms that suggest normal faulting. Moreover, although we have reason to believe that detachment faults are active in the Borrego area, few computed mechanisms have a nodal plane that is consistent with detachment faulting.

The interaction of secondary faults and master strands appears to be of prime importance in understanding earthquake nucleation processes in southern California. Earthquake swarms on secondary faults that occur prior to large events on master faults may be an important precursory signal in this and other tectonically complex regions. Other swarms that occur after large regional events probably indicate complex coupling and interaction of faults, possibly on detachments. Thus secondary faults may be an important aspect of earthquake hazard assessment, fault segmentation, and earthquake prediction.

Acknowledgments. This paper benefitted greatly by discussions with John Taber, John Beavan, Paul Huang, Cliff Thurber, Micky Van Fossen and Ken Howard. We also thank Diane Doser for her preprint and K. Nagao for drafting a figure. Critical reviews by Diane Doser, Allison Bent, C.H. Scholz and G. Bond improved the manuscript substantially. The staff of the Caltech Seismology Laboratory and USGS (Pasadena) are also thanked for providing the microearthquake data. This work was funded by USGS grant 14-08-001-G948. Lamont-Doherty Geological Observatory contribution 4829.

REFERENCES

Abe, K., Magnitudes of large shallow earthquakes from 1904 to 1980, *Phys. Earth and Planet. Inter., 27*, 72-92, 1981.

Allen, C.R., and J.M. Nordquist, Foreshock main shock, and larger aftershocks of the Borrego Mountain earthquake, *U.S. Geol Surv. Prof. Pap., 787*, 16-23, 1972.

Blom, R.G., R.E. Crippen, and E.G. Frost, Geometry and role of major east-dipping detachment faults in the initiation of the Salton Trough and localization of the San Andreas fault system, *Geol. Soc. Am. Abstr. Programs, 20*, A381, 1988.

Burdick, L.J., and G.R. Mellman, Inversion of the body waves from the Borrego Mountain earthquake to the source mechanism, *Bull. Seismol. Soc. Am., 66*, 1485-1499, 1976.

Clark, M.M., Surface rupture along the Coyote Creek fault, *U.S. Geol Surv. Prof. Pap., 787*, 55-86, 1972.

Crosson, R.S., Crustal structure modeling of earthquake data, 1, Simultaneous least squares estimation of hypocenter and velocity parameters, *J. Geophys. Res., 81*, 3036-3046, 1976.

Das, S., and C.H. Scholz, Off-fault aftershock clusters caused by shear stress increase?, *Bull. Seismol. Soc. Am., 71*, 1669-1675, 1981.

Dibblee, T.W., Jr., Geology of the Imperial Valley region, California, in Geology of Southern California, edited by R.H Jahns, *Calif. Div. Mines Bull. 170*, 21-28, 1954.

Dibblee, T. W., Jr., Stratigraphy and tectonics of the San Felipe Hills, Borrego Badlands, Superstition Hills, and vicinity, in The Imperial Basin -- Tectonics, Sedimentation, and Thermal Aspects, edited by C.A. Rigsby, Pacific Section, Society of Economic Paleontologists and Mineralogists, San Diego, Calif., vol. 40,31-44,1984.

Doser, D.I., Source characteristics of earthquakes along the southern San Jacinto and Imperial fault zones (1937 to 1954), *Bull. Seismol. Soc. Am., 80*, 1099-1117, 1990.

Doser, D.I., and H. Kanamori, Depth of seismicity in the Imperial Valley region (1977-1983) and its relationship to heat flow, crustal structure, and the October 15, 1979, earthquake, *J. Geophys. Res., 91*, 675-688, 1986.

Ebel, J.E., and D.V. Helmberger, P-wave complexity and fault asperities: The Borrego Mountain, California,

earthquake of 1968, *Bull. Seismol. Soc. Am., 72*, 413-438, 1982.
Engel, A.E.J., and P.A. Schultejann, Late Mesozoic and Cenozoic tectonic history of south central California, *Tectonics, 3*, 659-675, 1984.
Fisher, R.A., Dispersion on a sphere, *Proc. R. Soc. London, Ser. A, 217*, 295-305, 1953.
Fuis, G. S., W.D. Mooney, J.H. Healey, H.A. McMechan, and W. J. Lutter, Crustal structure of the Imperial Valley region, *U.S. Geol Surv. Prof. Pap., 1254*, 25-50, 1982.
Hamilton, R.M., Time-term analysis of explosion data from the vicinity of the Borrego Mountain, California, earthquake of 9 April, 1968, *Bull. Seismol. Soc. Am., 60*, 31-54, 1970.
Hamilton, R.M., Aftershocks of the Borrego Mountain earthquake from April 12 to June 12, 1968, *U.S. Geol. Surv. Prof. Pap., 787*, 31-54, 1972.
Heaton, T.H., and D.V. Helmberger, A study of the strong ground motion of the Borrego Mountain, California, earthquake of 1968, *Bull. Seismol. Soc. Am., 67*, 315-330, 1977.
Huang, P.Y., S.C. Solomon, E.A. Bergman, and J.L. Nábělek, Focal depths and mechanisms of Mid-Atlantic ridge earthquakes from body waveform inversion, *J. Geophys. Res., 91*, 579-598, 1986.
Hudnut, K.W. and M.M. Clark, New slip along parts of the 1968 Coyote Creek fault rupture, California, *Bull. Seismol. Soc. Am., 79*, 451-465, 1989.
Hudnut, K.W., and L. Seeber, Astroazimuth geodetic measurement of block rotation in the southern San Jacinto fault zone, California (abstract), *Eos Trans. AGU, 68*, 287, 1987.
Hudnut, K.W., L. Seeber, and J. Pacheco, Cross-fault triggering in the November 1987 Superstition Hills earthquake sequence, southern California, *Geophys. Res. Lett., 16*, 199-202, 1989a.
Hudnut, K.W., L. Seeber, and T. Rockwell, Slip on the Elmore Ranch fault during the past 330 years and its relation to slip on the Superstition Hills fault, *Bull. Seismol. Soc. Am., 79*, 330-341, 1989b.
Jones, L.M., Focal mechanisms and the state of stress on the San Andreas fault in southern California, *J. Geophys. Res., 93*, 8869-8891, 1988.
Kikuchi, M., and H. Kanamori, Inversion of complex body waves - II, *Phys. Earth Planet. Inter., 43*, 205-222, 1985.
Klein, F.W., Hypocenter location program, hypoinverse, part 1, *U.S. Geol Surv. Open File Rep., 78-694*, 1978.
Knopoff, L., Observation of silent earthquakes: The problem of intermittency of large earthquakes, paper presented at 25th General Assembly International Association of Seismology and Physics of the Earth's Interior, Istanbul, Turkey, Aug. 21-Sept. 1, 1989.
Louie, J., C. Allen, D. Johnson, P. Haase, and S. Cohn, Fault slip in southern California, *Bull. Seismol. Soc. Am., 75*, 811-833, 1985.
McCaffrey, R., Teleseismic investigation of the January 22, 1988 Tennant Creek, Australia, earthquakes, *Geophys. Res. Lett., 16*, 413-416, 1989.
McFadden, P.L., and F.J. Lowes, The discrimination of mean directions drawn from Fisher distributions, *Geophys. J. R. Astron. Soc., 67*, 19-33, 1981.
Nábělek, J.L., Determination of earthquake source parameters from inversion of body waves, Ph.D. thesis, 361 pp., Mass. Inst. of Technol., 1984.
Nicholson, C., L. Seeber, P. Williams, and L. Sykes, Seismic evidence for conjugate slip and block rotation within the San Andreas fault system, southern California, *Tectonics, 5*, 626-648, 1986.
Oppenheimer, D.H., W.H. Bakun, and A.G. Lindh, Slip partitioning of the Calaveras fault, California, and prospects for future earthquakes, *J. Geophys. Res., 95*, 8483-8498, 1990.
Plafker, G., and J.P. Galloway (Eds.), Lessons learned from the Loma Prieta, California, earthquake, *U.S. Geol. Surv. Circ., 1045*, 48 pp., 1989.
Rockwell, T., R. Blom, R. Crippen, R. Klinger, A. Stinston, and A. Thomas, Recognition, extension and significance of northeast trending faults between the Elsinore and San Jacinto fault zones using combined SPOT and LANDSAT imagery, Friends of the Pleistocene Fieldtrip Guidebook -- Western Salton Trough Soils and Neotectonics, 105-125, 1990.
Rogers, T.H., Geologic map of California, Santa Ana sheet, scale 1:250,000, Calif. Div. of Mines and Geology, Sacramento, 1985.
Sanders, C.O., Earthquake depths and the relation to strain accumulation and stress near strike-slip faults in southern California, *J. Geophys. Res., 95*, 4751-4762, 1990.
Sanders, C. O., and H. Kanamori, A seismotectonic analysis of the Anza seismic gap, San Jacinto fault zone, southern California, *J. Geophys. Res., 89*, 5873-5890, 1984.
Sanders, C. H. Magistrale, and H. Kanamori, Rupture patterns and preshocks of large earthquakes in the southern San Jacinto fault zone, *Bull. Seismol. Soc. Am., 76*, 1187-1206, 1986.
Savage, J., Dislocations in seismology, in *Dislocations in Solids*, vol. 3, edited by F.R.N. Nabarro, pp. 251-339, North Holland, New York, 1980.
Scheuing, D.F., and L. Seeber, Magnetic stratigraphy of the Ocotillo formation in the Borrego badlands segment of the San Jacinto fault zone, southern California and implications for block rotation, (abstract), *Eos Trans. AGU, 71*, 1311, 1989.
Seeber , L., and J.G. Armbruster, Stress orientation inferred from the kinematics of secondary faults within the San Andreas fault zone at Parkfield, (abstract), *Eos Trans. AGU, 69*, 1456, 1988.
Seeber, L., and C. Nicholson, Block fault rotation in geologic and interseismic deformation, in National Earthquake Prediction Council Special Report 1: Workshop on Special Study Areas in Southern California, edited by C. Shearer, *U.S. Geol. Surv. Open File Rep., 6-580*, 185-203, 1986.
Severson, L.K., Interpretation of shallow crustal structure of the Imperial Valley, California, from seismic reflection profiles, M.S. thesis, 68 pp., Lawrence Berkeley Lab., Univ. of Calif., Berkeley, 1987.
Sharp, R.V., Tectonic setting of the Salton Trough, *U.S. Geol. Surv. Prof. Pap., 787*, 3-15, 1972.
Simpson, D.W., W.S. Leith, and C.H. Scholz, Two types of reservoir-induced seismicity, *Bull. Seismol. Soc. Am., 78*, 2025-2040, 1988.
Sykes, L.R., and S.C. Jaumé, Seismic activity on neighboring faults as a long-term precursor to large earthquakes in the San Francisco Bay area, *Nature, 348*, 595-599, 1990.
Thatcher, W., and R.M. Hamilton, Aftershocks and source characteristics of the 1969 Coyote Mountain earthquake, San Jacinto fault zone, California, *Bull. Seismol. Soc. Am., 63*, 647-661, 1973.
Thatcher, W., J.A. Hileman, and T.C. Hanks, Seismic slip distribution along the San Jacinto fault zone, southern California and its implications, *Geol. Soc. Am. Bull., 86*, 1140-1146, 1975.
Turcotte, D.L., and G. Schubert, *Geodynamics: Applications of Continuum Physics to Geological Problems*, 450 pp., John Wiley, New York, 1982.
Walcott, R.I., Structure of the earth from glacio-isostatic rebound, *Annu. Rev. Earth Planet. Sci., 1*, 15-37, 1973.
Wyss, M., and T.C. Hanks, Source parameters of the Borrego Mountain earthquake, *U.S. Geol. Surv. Prof. Pap., 787*, 24-30, 1972.

J.G. Armbruster and Leonardo Seeber, Lamont-Doherty Geological Observatory of Columbia University, Palisades, NY 10964.

K.W. Hudnut, Seismological Laboratory, California Institute of Technology, Pasadena, CA 91125.

J.L. Nábělek, College of Oceanography, Oregon State University, Corvallis OR 97331.

J. Pacheco, M.D. Petersen, and Lynn R. Sykes, Department of Geological Sciences and Lamont-Doherty Geological Observatory of Columbia University, Palisades, NY 10964.

(Received November 28, 1990;
revised April 4, 1991;
accepted May 6, 1991.)